Journal of Catalysis 377 (2019) 199–208

Contents lists available at ScienceDirect

Journal of Catalysis

journal homepage: www.elsevier.com/locate/jcat

# Metal-free carbocatalyst for catalytic hydrogenation of N-containing unsaturated compounds

Zhaolin He [a], Jin Liu [a], Qijun Wang [b], Meng Zhao [a], Zhipan Wen [a], Jun Chen [a], Devaraj Manoj [b], Chuyi Xie [b], Jiangbo Xi [a,*], Junxia Yu [a,*], Chunyan Tang [c], Zhengwu Bai [a], Shuai Wang [b]

[a] School of Chemistry and Environmental Engineering, Wuhan Institute of Technology, Wuhan 430073, China
[b] Key Laboratory of Material Chemistry for Energy Conversion and Storage, Ministry of Education, School of Chemistry and Chemical Engineering, Huazhong University of Science and Technology, Wuhan 430074, China
[c] School of Computer, Electronics and Information in Guangxi University, Nanning, 530004 Guangxi, China

ARTICLE INFO

*Article history:*
Received 14 May 2019
Revised 7 July 2019
Accepted 10 July 2019

*Keywords:*
Carbocatalyst
Nitrogen doped holey graphene
Hydrogenation
Organic dye
Density functional theory

ABSTRACT

Eco-friendly carbocatalyst is extremely desirable in organic catalysis and wastewater treatment. Herein, we reported a one-pot synchronous hydrothermal process to synthesize a highly efficient N doped holey graphene (NHG) carbocatalyst, in which graphene oxide nanosheets are self-assembled, reduced, chemically etched, and simultaneously doped with nitrogen to form a graphene hydrogel in the presence of $H_2O_2$ and $NH_4OH$. Benefiting from the good hydrophilicity, unique hierarchical porous structure, large specific surface area (322.1 $m^2 g^{-1}$), and high N content (9.77 at. %), the resultant NHG carbocatalyst exhibits an excellent catalytic performance for the hydrogenation of N-containing unsaturated compounds. In 4-nitrophenol reduction reaction, the NHG carbocatalyst delivers a turnover frequency of $3.32 \times 10^{-2}$ - $min^{-1}$. This catalytic activity is superior to that of the commercial Pd/C (5.0 wt%), other previously reported carbocatalysts, and many noble-metal-based catalysts. Furthermore, the molecular structure analysis combined with density functional theory calculations elucidate metal-free catalytic mechanism of hydrogenation reaction for unsaturated chromophore groups in N-containing organic dyes.



## 1. Introduction

As a major source of water pollution, toxic organic dyes from manufacturing process, such as textiles, foods, drugs and cosmetic industry activities, have become a global concern due to their non-biodegradation, environmental persistence and bio-accumulation, thus leading to adverse ecological impact in living organisms [1–3]. Organic synthetic dyes have reactive functional groups such as nitro- (O ← N═O), azo (—N═N—) and imine (—C═N—) moieties along with heterocyclic and aromatic rings in their structures. Therefore, it is necessary to cleave these unsaturated chromophore groups of these toxic dyes by decolorization, and finally to convert them into nontoxic forms [4–6]. In environmental catalysis industry, most of the homogeneous and heterogeneous catalytic conversions are mainly based on either noble [7,8], transition [9–11] and rare-earth metals or their oxides [12,13]. However, these metal-based catalysts have numerous drawbacks, such as scarcity, high cost, deactivation, and secondary pollution in the disposal of waste catalysts, which raised the questions in terms of sustainable development [14]. In order to solve above-mentioned issues associated with metal-based catalyst, exploring and developing novel metal-free materials as alternatives to metal-based catalysts, is of growing scientific and technological importance [15–17]. Moreover, metal-free catalysts can provide more beneficial effects as of non-secondary contamination for environmental catalysis, especially in water/wastewater remediation [18]. In this regard, carbocatalysts have captured profound attention in metal-free catalysis due to their wide availability, environmental acceptability, low-cost, stability/recyclability, and sustainable properties [19,20]. Unfortunately, environmental catalysis process of carbocatalyst have not been intensively investigated, and therefore related research is still in the early stages of development [21,22].

As one of the most promising carbocatalysts, graphene-based materials are endowed with excellent catalytic performance due to their large specific surface area, high conductivity as well as excellent corrosion resistant property. Particularly, their catalytic activity can be dramatically enhanced by doping foreign atoms into the graphene lattice and thus modulate the electronic and chemical properties [23,24]. Chen and coworkers reported the metal-free catalytic reduction of 4-nitrophenol (4-NP) to 4-aminophenol (4-AP) mediated by N doped graphene (NG). Their theoretical

* Corresponding authors.
*E-mail addresses:* jbxi@wit.edu.cn (J. Xi), yujunxia_1979@163.com (J. Yu).

https://doi.org/10.1016/j.jcat.2019.07.017
0021-9517/

calculations further demonstrated that the C atoms next to the doped N atoms can be activated, leading to a higher positive charge density [25]. The drastic enhancement in catalytic behavior is attributable to the electronegativity of doped heteroatoms, which break carbon's electroneutrality *via* induced effect, and consequently create catalytic sites. In our previous work, the reduction reaction of 4-NP catalyzed by N/P dual doped graphene (NPG) was also examined. Attributed to the co-doping of N and P atoms, the resultant NPG carbocatalyst exhibited excellent catalytic performance for 4-NP reduction. In addition, the remarkable catalytic activity of NPG can also be extended to the reduction of various substituted nitrobenzenes [26] Generally, heteroatoms are usually introduced into graphene frameworks through post-treatment of graphene-base materials (eg. Graphene oxide (GO), exfoliated graphene) with heteroatom-containing precursors [27,28]. In fact, the homogeneous doping of heteroatoms in graphitic structure remains a formidable challenge, because it is difficult to accurately control the dopant content and doping sites in graphene. As a rule, the amount of catalytic sites and the accessibility of the reactants to active sites are essential for activity of the catalyst. Therefore, the graphene materials with high doping content and porous structure are highly desirable, because they can offer high density of exposed active surface and diffusion channel for efficient catalytic processes.

In this work, we describe the development of an efficient N doped holey graphene (NHG) carbocatalyst, using GO as a starting material, hydrogen peroxide ($H_2O_2$) as etching agent and ammonium hydroxide ($NH_4OH$) as nitrogen sources *via* a facile one-pot hydrothermal synthesis route. Due to high N doping content and porous structure, the as-prepared NHG demonstrates enhanced catalytic activity and excellent dispersible property in water. In aqueous solution, NHG is employed as an efficient carbocatalyst and exhibits an excellent organocatalytic activity, high stability, selectivity and good recyclability for the hydrogenation of organic dyes and nitrobenzenes. Furthermore, the molecular structure analysis combined with density functional theory (DFT) calculations elucidate metal-free catalytic mechanism of hydrogenation reaction for unsaturated chromophore groups in N-containing organic dyes.

## 2. Experimental section

### 2.1. Materials

Ammonium hydroxide ($NH_4OH$), hydrogen peroxide ($H_2O_2$), Nitrobenzene, 4-nitrotoluene, 4-chloronitrobenzene, 4-bromonitrobenzene, 4-nitrobenzoic acid, 4-nitrobenzonitrile, 4-nitrophenol (99%) and sodium borohydride (96%) were purchased from Sinopharm Chemical Reagent Co., Ltd. (Shanghai, China). Pd/C (5 wt%) were purchased from Aladdin Chemistry Co., Ltd. (China)., methylene blue (MB), methylene orange (MO), rhodamine B (RhB) and Congo red (CR) were purchased from Sinopharm Chemical Reagent Co., Ltd. (Shanghai, China), and the rest of the chemicals were procured from Sigma-Aldrich. Deionized water (resistivity > 18 $\Omega \cdot cm^{-1}$) was used for all syntheses and experiments.

### 2.2. Instrumentation

The morphology of the synthesized NHG catalyst was characterized using a FEI Nova NanoSEM 450 scanning electron microscope (SEM). Transmission electron microscopy (TEM) and high-resolution transmission electron microscopy (HRTEM) images were obtained using a TECNAI G2 20 U-Twin instrument (Netherlands) operated at an acceleration voltage of 200 kV. The samples for SEM characterization were prepared by drop-casting the sample suspensions (dispersed in ethanol, 1 mg/mL) on pre-cleaned silicon wafers. For TEM, 5 μL of the sample suspensions (dispersed in ethanol, 0.5 mg/mL) were drop-casted on a carbon-coated copper grid. X-ray photoelectron spectroscopy (XPS) was performed with an ESCALAB MKII spectrometer (VG Co., UK), using Mg Kα radiation (1253.6 eV) at a pressure of $2.0 \times 10^{-10}$ mbar. The peak positions were internally referenced to the C 1s peak at 284.6 eV. Raman spectrum was measured by a confocal laser micro-Raman spectrometer (DXR, USA) equipped with a He–Ne laser of excitation of 532 nm at a laser power of 0.6 mW. Nitrogen adsorption/desorption isotherms were obtained at 77 K on an accelerated surface area and porosimetry system (ASAP 2020, Micromeritics, USA) to measure the surface area of the material using the Brunauer-Emmett-Teller (BET) method. The UV–vis measurements of the synthesized NHG carbocatalyst along with the time-dependent kinetic spectra during catalysis were performed on a UV-2550 spectrophotometer (Shimadzu, Japan). High-performance liquid chromatography (HPLC) analysis was performed on an Agilent-1100 system with a Zorbax Eclipse XDB-C18 4.6 × 150 mm column (Agilent, USA). The MALDI–ultra-high resolution MS of reduced product was performed using a solariX 7.0 T FTICR mass spectrometer (Bruker Daltonics, Germany). The reduced product was determined by the integrals in $^1H$ NMR spectrum which was measured with a NMR 400 MHz spectrometer (Varian, USA). The sample solution (20 mg/ml) of reduced product was prepared with deuterated $CDCl_3$ as the solvent.

### 2.3. Synthesis of NHG carbocatalyst

GO aqueous solution was initially prepared by the modified Hummers method [29]. As-prepared GO solution (30 mL, 8.0 wt%) was diluted by 30 mL water by a sonication process. To the above prepared mixture, 15 mL of $NH_4OH$ (28 wt%) and 7 mL of $H_2O_2$ (0.3 wt%) was injected rapidly under stirring. Subsequently, the mixture was transferred into a 100 mL Teflon-lined autoclave and heated at 180 °C for 8 h. During this hydrothermal process, GO nanosheets were reduced and self-assembled to form a monolithic hydrogel. At the same time, reduce GO nanosheet was also etched by $H_2O_2$, and was doped with N atoms in the graphene framework. The obtained NHG hydrogel was soaked in deionized water and washed for several times to remove residual $NH_4OH$. Finally, the NHG hydrogel was immersed in *ca.* 100 mL water, followed by pulverization *via* an ultrasonic disintegrator for a period of 3 h, and a homogeneous NHG suspension can be obtained. The concentration of the NHG suspension was measured via freeze-drying before use. For comparison, NG and holey graphene (HG) were also prepared by the same process without the adding $H_2O_2$ and $NH_4OH$, respectively.

### 2.4. Catalytic reduction of N-containing unsaturated compounds

In a typical catalysis reaction, 1 mL of NHG suspension (2.7 mg/mL) was injected into 3 mL aqueous solution with 4-NP (20 mM) and $NaBH_4$ (2 M). Then the reaction mixture was thoroughly mixed under magnetic stirring at room temperature. The reaction process was monitored by thin-layer chromatography (TLC) in regular intervals. After completion of the reaction, the reaction solution was analyzed with UV/Vis detection or HPLC measurement after filtering off the catalyst. Decrease in extinction intensity with time was measured at maximum absorbance values (λ max), the λ max = 400 nm, 465 nm, 498 nm, 554 nm and 665 nm for 4-NP, MO, CR, RhB and MB, respectively.

### 2.5. Computational methodology

All the DFT calculations of the 5 organic dyes were carried out by using Gaussian 09 program package [30]. The molecular structures of these 5 dye molecules were fully optimized in vacuum by a standard 6-31G (d, p) set with B3LYP functional without considering the solvent. C, H, N, O, S and Na were described by C, H, N, O, S and Na [31–33]. Vibrational frequencies were calculated for all stationary points at the same level to verify whether the each was a minimum (NIMAG = 0) on the potential energy surface.

## 3. Results and discussion

### 3.1. Synthesis and characterizations of materials

The preparation involves a facile one-pot method by hydrothermal treatment of GO in the presence of $NH_4OH$ and $H_2O_2$ (Fig. 1A). During this process, GO nanosheets were self-assembled to realize a black monolithic graphene hydrogel (Fig. 1B). At the same time, GO was also reduced, chemically etched to form pore openings on conjugated carbon surface *i.e.*, holey reduced graphene oxide (RGO) and simultaneously doped with nitrogen. As can be seen from the SEM image, the NHG hydrogel exhibit a 3D network with highly interconnected sheets, which are interlocked together and prevented them from restacking to maintain a highly macroporous framework (Fig. 1C and 1D).

The fine structural properties were further characterized by TEM and dark field scanning TEM (DF-STEM) images. Fig. 2A and 2B indicate the existence of small pores in the surface of graphene nanosheets. From higher magnification TEM image, it further confirms the presence of tiny pores with 2–4 nm in size, and are distributed on the basal plane of graphene nanosheets (Fig. 2C). There is an obvious contrast between the mesoporous surface in NHG and intact ones of hydrothermally treated graphene without $H_2O_2$ (Fig. 2D), indicating the successful etching of graphene sheets on the surface. The distributions of C, O and N in NHG are almost

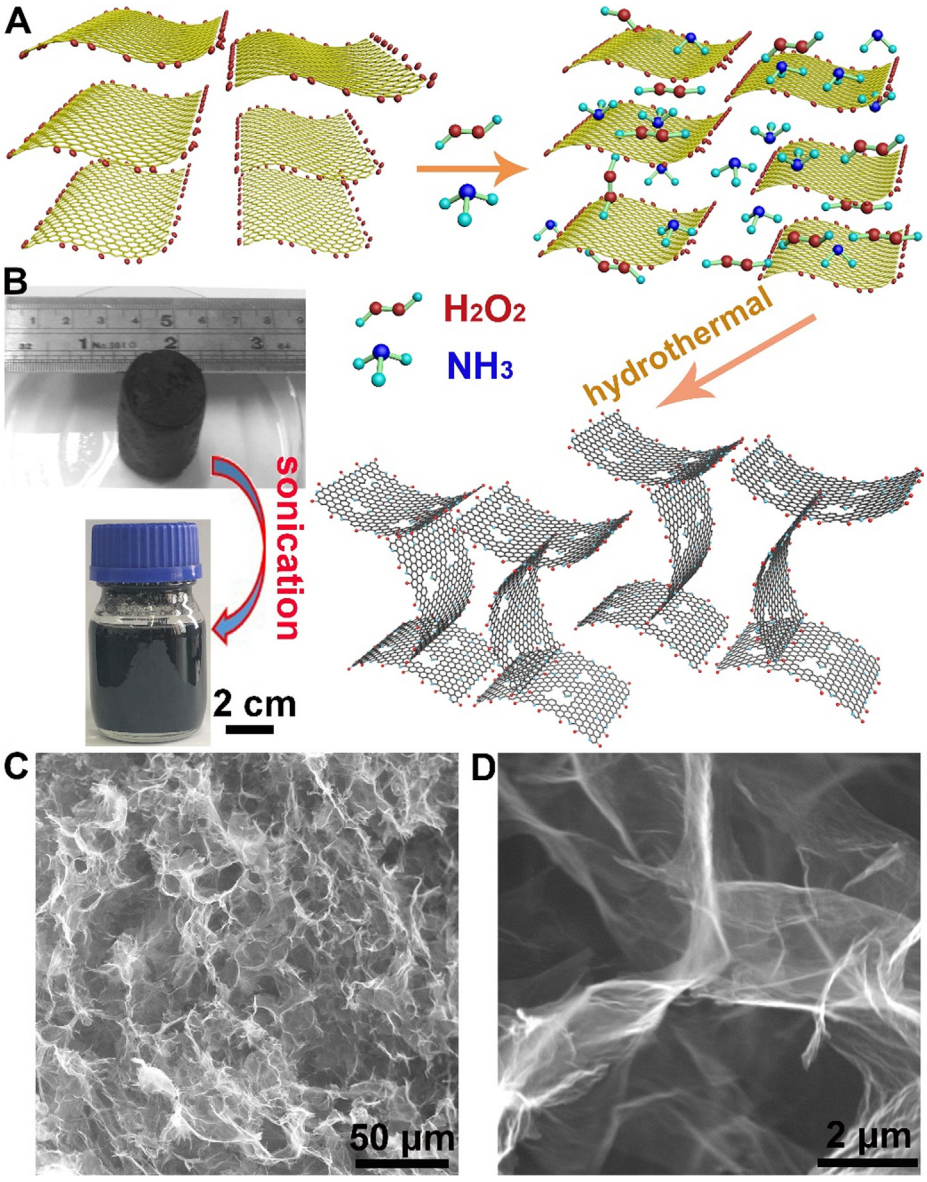


**Fig. 1.** (A) Schematic illustration of the fabrication of the NHG. (B) Photograph of NHG hydrogel and aqueous dispersion; (C) The typical SEM image of the NHG hydrogel (bottom left) reveals a 3D porous configuration with interconnected pores ranging from sub-micrometers to several micrometers; and (D) High resolution SEM image of NHG.

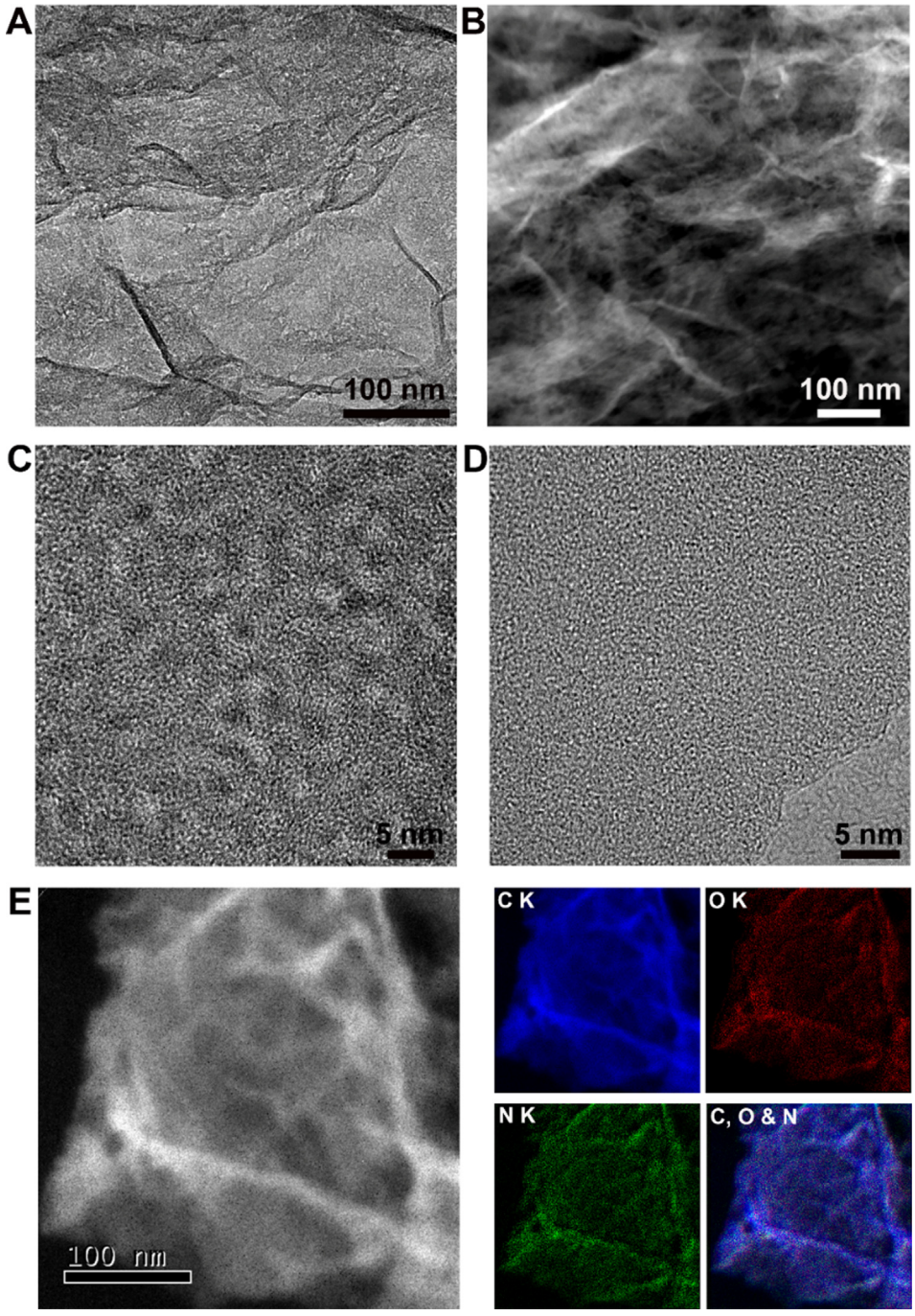


**Fig. 2.** (A) High-magnification bright-field TEM image of NHG; (B) DF-STEM image of NHG. (C) TEM images of NHG in comparison to (D) pore-free NG. (E) STEM image and elemental mapping of C, O, and N for NHG.

overlap with each other according to the element mappings in Fig. 2E, confirming the homogeneous doping of N atomic species in NHG.

To gain further insight of content and chemical status of elements in NHG, XPS analysis were carried out. As can be seen in Fig. 3A, the peaks located at *ca.* 285, 400, and 532 eV correspond to $sp^2$ hybridized carbon 1 s, dopant nitrogen 1 s, and oxygen 1 s, respectively, which is in accordance with the elemental mapping analysis. The atomic percentage of N in the HNG is calculated to be 9.77 at. %, which is much higher than that in pore-free NG (6.13 at. %) as shown in Fig. 3A Inset. This high doping degree should be attributed to the defects of the holey structure that facilitates the doping of heteroatoms [34]. As depicted in Fig. 3B, there are three components in the C 1s spectrum of the HNG. The strong signal at 285.0 eV can be assigned to the graphite-like $sp^2$ carbon, indicating most of the C atoms in the HNG are arranged in a conjugated honeycomb lattice even when the doped N is high up to 9.77 at. %. The weak peaks at 285.7 and 287.4 eV reflect different bonding structure of the C-N bonds, corresponding to the N-$sp^2$ C and N-$sp^3$ C bonds, respectively, and would originate from either substitution of N atoms, defects or the edge of the graphene nanosheets [35]. The N 1s peak can be deconvoluted into four single peaks, indicating that N atoms are in the four different bonding characters doped into the graphene framework (Fig. 3C).

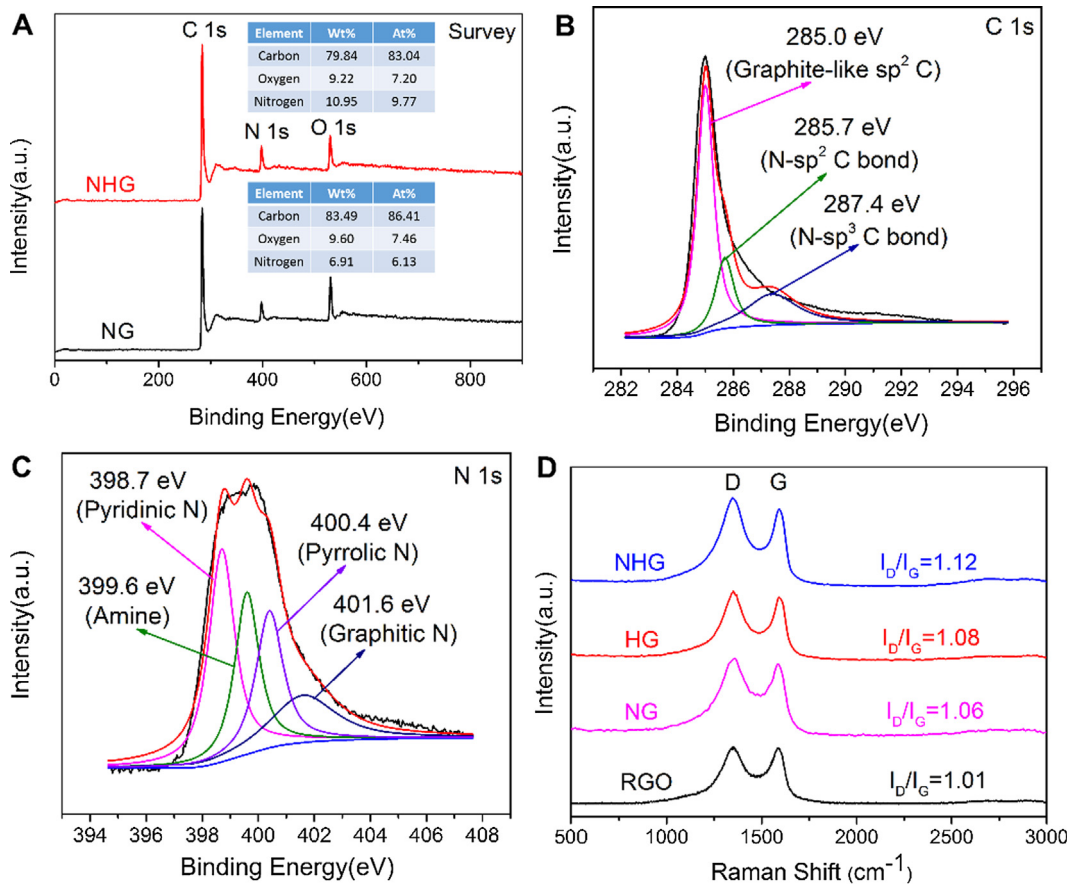


**Fig. 3.** (A) XPS survey spectrum of NHG and NG, the according elemental analysis is shown in the inset. (B) High-resolution XPS spectrum of C 1s, and (C) High-resolution XPS spectrum of the N 1s peak, (D) Raman spectra of NHG in comparison to N-free HG and pore-free and RGO.

These four kinds of doped N atoms are located at *ca.* 398.7, 399.6, 400.4 and 401.6 eV, corresponding to pyridinic, amine, pyrrolic and graphitic configurations, respectively [25]. The peak intensity for "pyridinic", "amine" and "pyrrolic" N is much higher than that of "graphitic" N, thus it clearly evidences N atoms should be mainly substitutionally doped into the graphene lattice at the edge of graphene nonosheets and inner boundary of holes in holey graphene, where oxygen-containing functional groups are rich. This result is in consistent with Dai group's findings that N-doping depend on the amounts of these oxygen functional groups at the defect and edge sites of graphene using ammonia as nitrogen source [36].

Raman spectroscopy measurements have also been applied to investigate the structural defects in HNG and control samples. The typical D band located at around 1350 $cm^{-1}$ representing the edges, defects and disordered carbon sites, and the G band centered at 1580 $cm^{-1}$ assigning to the in-plane bond-stretching motion of pairs in $sp^2$-C atoms [37]. Therefore, in the Raman spectra, a larger ratio of the D band and G band ($I_D/I_G$) intensity for graphene materials usually indicates a higher content of disordered carbon and defect level. As shown in Fig. 3D, the intensity ratio ($I_D/I_G$) for HNG, HG, NG and RGO are calculated as 1.12, 1.08, 1.06 and 1.01, respectively, the higher intensity ratio observed at HNG is attributed to the holey structure and N doping in graphene framework. These intrinsic properties may further interrupted the graphitic carbon configuration as well as electronic structure of graphene and result in high dense of defective sites [38].

$N_2$ adsorption-desorption isotherms and pore-size distribution of NHG and pore-free NG are shown in Fig. 4. The as-prepared HNG (freeze-dried) exhibits a specific surface area (SSA) of 322.1 $m^2\ g^{-1}$ (Fig. 4A), much higher than that of NG (108.9 $m^2\ g^{-1}$) (Fig. 4C). In addition, these two samples possess a mesoporous structure according to the pore-size distribution curves (Fig. 4B and 4D). Meanwhile, the curves in Fig. 4B demonstrate that HNG possess a wider pore-size distribution (2–4 nm) compare with NG (centered at *ca.* 4 nm) (Fig. 4D). This observations are also confirmed by HRTEM images as shown in Fig. 2. Therefore, the higher specific surface area and wider pore-size distribution of HNG are attributed to the holey structure coursed by $H_2O_2$ etching. These marcoporous structure and mesoporous graphene nanosheets are expected to facilitate the exposure of active sites, enhance the diffusion of reactants in organocatalysis process.

### *3.2. Evaluation of catalytic performance of synthesized NHG toward the hydrogenation of organic dyes*

The catalytic performance of NHG was further evaluated by investigating the hydrogenation reaction of five common organic dyes (4-NP, MO, CR, RhB and MB) in aqueous solution, using $NaBH_4$ as a reducing agent at room temperature (Fig. 5A and Fig. S1). Due to the excellent hydrophilic nature, NHG can be well dispersed in aqueous media (Fig. 1B), consequently leading to sufficient exposure and easier access of active sites to the reactants during the reaction. The catalytic decolorization processes of these dyes were monitored by the color bleaching of dye solution after the addition of an excess amount of $NaBH_4$ and NHG carbocatalysts, as indicated by the gradual decrease in the maximum absorbance values with time in the UV–vis spectra [5,39,40]. As shown in Fig. 5B-F, the adsorption peak at λ max gradually decreases with respect to reaction time, indicating the reduction of these 5 dyes occur in the presence of NHG carbocatalyst (40 s, 9 min, 2 min, 3 min, and

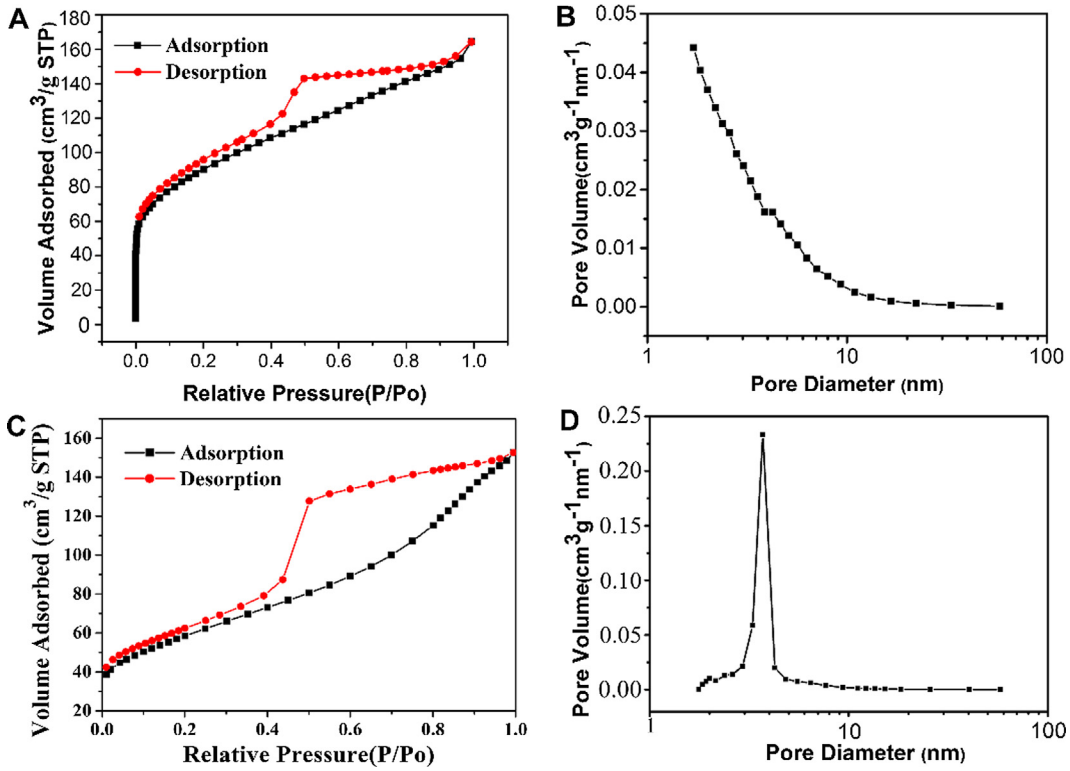


**Fig. 4.** (A) Nitrogen adsorption/desorption isotherms of the NHG and (B) DFT pore-size distribution of NHG. (C) Nitrogen adsorption/desorption isotherms of the pore-free NG and (D) DFT pore-size distribution of NG.

11 min for 4-NP, MO, CR, RhB and MB, respectively). To clarify the catalytic effect of NHG, our extensive detection excludes the presence of adsorbed dyes in the ethanol extraction solution of used NHG carbocatalyst. No absorbed dye was extracted, further confirming the complete decolorization. Herein, the reduction of 4-NP is chosen as a model reaction to evaluate the catalytic activity of NHG. The bright yellow colored aqueous mixture of 4-NP/$NaBH_4$ presents a maximum absorption band at 400 nm due to the formation of dark 4-nitrophenolate ions [41]. The color of 4-nitrophenolate completely fade within 40 s (Fig. 5B). Additionally to the absorption band at 300 nm, the reaction solution presents an absorption band at 230 nm associated to the aromatic group, corresponding to the formation of 4-AP [42]. A high excess of $NaBH_4$ was employed to ensure that its concentration remained essentially constant during the whole reaction, which allowed the assumption of pseudo-first-order kinetics with respect to the substrates. Thus the catalytic efficiency can calculated by turnover frequency (TOF), which is defined as the amount of 4-NP molecules that 1 mg catalyst can convert into 4-AP per min (calculation formula). As a result, the TOF of NHG is calculated to be $3.32 \times 10^{-2}$, which is superior to that of other carbocatalysts, commercial Pd/C (5.0 wt%), and many noble-metal-based catalysts reported previously (Table 1). By comparison, NG and HG were also used as catalysts for 4-NP reduction. 4-NP aqueous solutions (0.06 mmol) can be completely reduced within 80 s in the presence of NG (Fig. S2), while HG just exhibited a low adsorption capacity and no 4-AP was detected from UV/Vis analysis (Fig. S3). These findings demonstrate that the enhanced catalytic activity should originate from N doping and hierarchical porous structure of the graphene frameworks. Furthermore, the recyclability of the NHG carbocatalyst was also investigated by repeated uses of the recycled catalyst in the same condition. In each cycle, NHG was recovered from the reaction mixture by filtration *via* a disassembling filter and subsequently washed with ethanol and deionized water subsequently. Notably, a 92% conversion was maintained even in the eighth run (Fig. S4), revealing an excellent durability of NHG carbocatalyst.

$$\text{TOF } (min^{-1}) = \frac{mmoles\ of\ 4-NP\ converted\ per\ minute}{\text{mg of catalyst}}$$

(Calculation formula of TOF)

### 3.3. Evaluation of catalytic performance of NHG carbocatalyst toward nitrobenzenes (Ar-$NO_2$) reduction

On the basis of the results, we further extended the NHG carbocatalyst to the reduction reactions of various substituted nitrobenzenes to examine its common applicability. Due to the poor solubility of nitrobenzene or substituted nitrobenzenes in water, $H_2O$/ethanol mixture was used as their solvent for the catalytic process. The According to the data are summarized in Table 2, nitrobenzenes can be reduced into anilines by $NaBH_4$ in $H_2O$/ethanol mixture in the presence of NHG carbocatalyst. It should be noted that the reaction efficiency in $H_2O$/ethanol mixture was lower than that in water. As a result, the different molecular structure and reaction conditions should be ascribe to the different behavior of reduction of 4-NP (40 s) compared to all others nitrobenzenes systems (5–20 min).

### 3.4. Mechanism investigation of hydrogenation azo (—N=N—) and imine (—C=N—) catalyzed by NHG carbocatalyst

Based on these considerations, the catalytic centers of NHG in activation of hydrogenation should originate from the created defective sites due to nitrogen atoms are incorporated into the porous graphene framework. The existence of nanoholes in the basal plane of NHG not only provides a "short-cut" for efficient mass transport, but also provides more exposed active sites due to

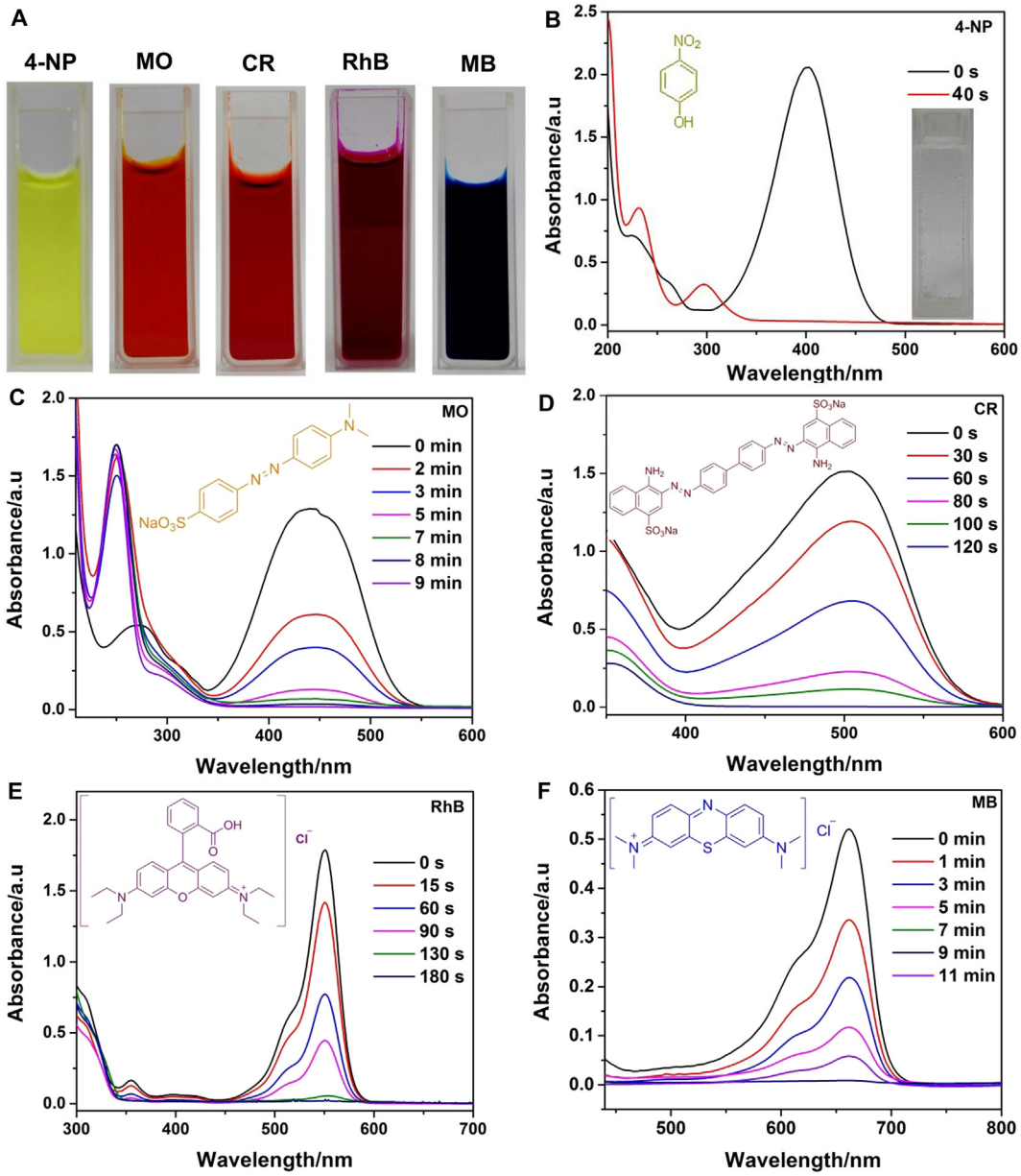


**Fig. 5.** (A) Photograph of the five common organic dyes (4-NP, MO, CR, RhB and MB) in aqueous solution; Time-dependent absorption spectra showing the hydrogenation of 4-NP (B), MO (B), CR (C), RhB (D) and MB (F) using NHG as metal-free catalyst in the presence of $NaBH_4$, insets are structural formula of the corresponding dye molecules. The inset of Fig. 5B is the photograph of the reduced 4-NP solution.

increased edges [53]. In addition, we explored its innovative application in the catalytic hydrogenation reaction of azo (—N=N—), imine (—C=N—). These two hydrogenation reactions catalyzed by metal-free carbocatalyst has never been reported previously. Therefore, little attention has been devoted to the metal-free catalytic mechanism of hydrogenation reaction for azo and imine. To gain further understood about the metal-free catalytic process, the reaction mechanism is elucidated by molecular structure analysis and DFT calculations. The molecule structure of hydrogenation product of MO was identified from mass and $^1H$ NMR spectra. As shown in Figs. S5 and S6, N, N-dimethyl-p-phenylenediamine ($C_8H_{12}N_2$) was obtained after reduction, indicating the cleavage of —N=N— bond in MO and resulted in formation of amino-group. In addition, we also tried to obtain the products of hydrogenated imine via extraction. Unfortunately, colorless Leuco MB is very readily oxidized back to blue MB by oxygen in the process of rotary evaporation even at room temperature, which is in agreement with previously reported work [54]. Similar phenomenon was also observed for the RhB because of the same chromophore group as MB was contained in RhB molecular structure. Therefore, we failed to analyze the molecule structures of hydrogenated MB and hydrogenated RhB.

In order to elucidate the catalytic effect on dyes hydrogenation of NHG, DFT along with time dependent DFT calculations were performed to investigate the density of states (DOS), charge density, electrostatic potential distribution and UV–vis spectra. As can be seen from Fig. 6A, compared with NG, NHG shows a significantly increase of DOS near the Fermi level due to its holey structure. This will bring NHG a superior electrical conductivity to NG, which can facilitate the electron transfer and finally improve the hydrogenation activity of NHG. The charge density mapping diagram shows that N atom possess a high charge density (inset in Fig. 6A), which play an important role to create catalytically active sites in their neighboring C atoms. Therefore, the activated C sites bear more

**Table 1**
The comparison of catalytic activity of NHG and other metal-free carbocatalysts or noble metal based catalysts for 4-NP reduction.

| Catalyst | Mass of catalyst (mg) | Amount of 4-NP (mmol) | Conversion time (min) | TOF (mmol 4-NP/(mg cat.· min) | *Ref.* |
|---|---|---|---|---|---|
| NHG | 2.7 | $6 \times 10^{-2}$ | 0.67 | $3.32 \times 10^{-2}$ | a |
| NG | 2.0 | $6 \times 10^{-2}$ | 1.33 | $2.26 \times 10^{-2}$ | a |
| Pd/C (wt.5%) | 2.0 | $6 \times 10^{-2}$ | 1.10 | $2.73 \times 10^{-2}$ | a |
| N,P dual-doped graphene | 1.0 | $6 \times 10^{-2}$ | 2.53 | $2.37 \times 10^{-2}$ | [26] |
| S, N co-doped carbon nanotubes | 0.0093 | $2 \times 10^{-4}$ | 10 | $2.15 \times 10^{-3}$ | [43] |
| N-doped graphene | 2.0 | $5 \times 10^{-1}$ | 120 | $2.08 \times 10^{-3}$ | [44] |
| N-doped graphene | 0.137 | $1.76 \times 10^{-4}$ | 21 | $6.05 \times 10^{-5}$ | [25] |
| AA/GO | 2.5 | $5 \times 10^{-4}$ | 80 | $2.5 \times 10^{-6}$ | [45] |
| pH-mediated graphene | 2.5 | $5 \times 10^{-4}$ | 60 | $3.33 \times 10^{-6}$ | [46] |
| $Fe_3O_4$@P(MBAAm-*co*-MAA)@Ag | 2 | $4 \times 10^{-2}$ | 0.75 | $2.67 \times 10^{-2}$ | [47] |
| RGO@AC/Pd | 1.0 | $3 \times 10^{-2}$ | 1.65 | $1.8 \times 10^{-2}$ | [9] |
| CMF@PDA/Pd | 492 | $1 \times 10^{-2}$ | 0.25 | $8.13 \times 10^{-5}$ | [48] |
| NCT@Pd | 1 | $6 \times 10^{-4}$ | 0.67 | $9 \times 10^{-4}$ | [49] |
| Fe@NC@Pd | 2 | $3 \times 10^{-2}$ | 1.92 | $7.8 \times 10^{-3}$ | [50] |
| ASNTs@Pd | 2 | $6 \times 10^{-2}$ | 0.67 | $4.48 \times 10^{-2}$ | [51] |
| Pd-rGO-CNT | 5 | $3 \times 10^{-4}$ | 0.33 | $3.03 \times 10^{-4}$ | [52] |

[a]This work.

**Table 2**
Catalytic reduction of nitrobenzene and substituted nitrobenzenes into amines by $NaBH_4$ catalyzed by NHG carbocatalyst[a].

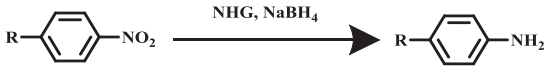


| Entry | Reactant | Product | *T* (min) | Yield (%)[b] |
|---|---|---|---|---|
| 1 | 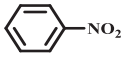 | 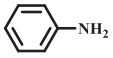 | 15 | 99.1 |
| 2 | 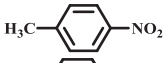 | 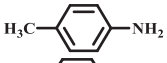 | 20 | 98.9 |
| 3 | 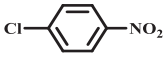 | 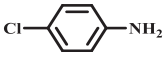 | 7 | 99.0 |
| 4 | 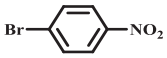 | 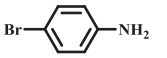 | 5 | 99.1 |
| 5 | 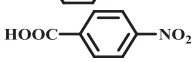 | 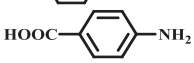 | 5 | 95.0 |
| 6 | 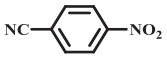 |  | 7 | 93.6 |

[a] Standard reaction conditions: 0.06 mmol nitrobenzene or substituted nitrobenzenes, 2.7 mg NHG, 3 mL $H_2O$/ethanol = 1/9 (v/v), and 6 mmol (100 equiv.) $NaBH_4$ at room temperature.
[b] HPLC content.

positive charge and thus enhance the H ions transfer during the hydrogenation reaction of organic dyes [25]. We also examined the cleave reaction process of unsaturated chromophore group by calculating the electrostatic potential distributions of these 5 organic dyes. Fig. 6B–F show that the —N=N— or —C=N— bonds areas (orange and red areas) have lower charge density than other area in the molecules. As a result, these N-containing unsaturated chromophore groups should be low electrostatic potential sites, and thus can be considered as the potential reactive site during the hydrogenation process. These consequences clearly indicate that the partially negative charged N atoms in NHG are act as the adsorb sites to interact with the low electrostatic potential sites in organic dyes and result in corresponding hydrogenated products. Based on the experimental results and the theoretical calculations, a reasonable explanation for the metal-free catalytic mechanism can be proposed. The catalytic behavior may occur in three steps: (1) in aqueous solution, $BH_4^-$ ions interact with the activated C atoms in NHG and dye molecules diffused/adsorbed onto NHG *via* electrostatic interaction between the partially negative charged N sites and N-containing unsaturated chromophore groups (low electrostatic potential sites), (2) dye molecules capture the reductive H species as soon as they contacted with the active sites, leading to the hydrogenation of N-containing unsaturated chromophore groups, and (3) the hydrogenated products desorbed from the active sites.

In addition, the frontier orbitals along with UV–vis spectra of the hydrogenated products are also calculated in Fig. S7. As shown in Fig. S7A–6E, the modulated UV–vis spectra match well with the experimental results, which provide extra evidence for the correctness of the structure of target products. The corresponding inset HOMO and LUMO orbitals of five products indicates that charge transfer can be ascribed to the inter-molecular charge transfer process. This process may further result in the higher HOMO/LUMO energy gap, and thus lead to the blue shift of maximum absorption wavelength (<400 nm). Furthermore, the 1 s orbitals of N atoms in NHG owns more partial density of states (PDOS) than that in NG (Fig. S7F), which is consistent with the calculated total DOS in Fig. 6A. The above calculation results demonstrate that graphene with holey structure and nitrogen atoms doping can act as the efficient material for the catalytic hydrogenation of organic dyes.

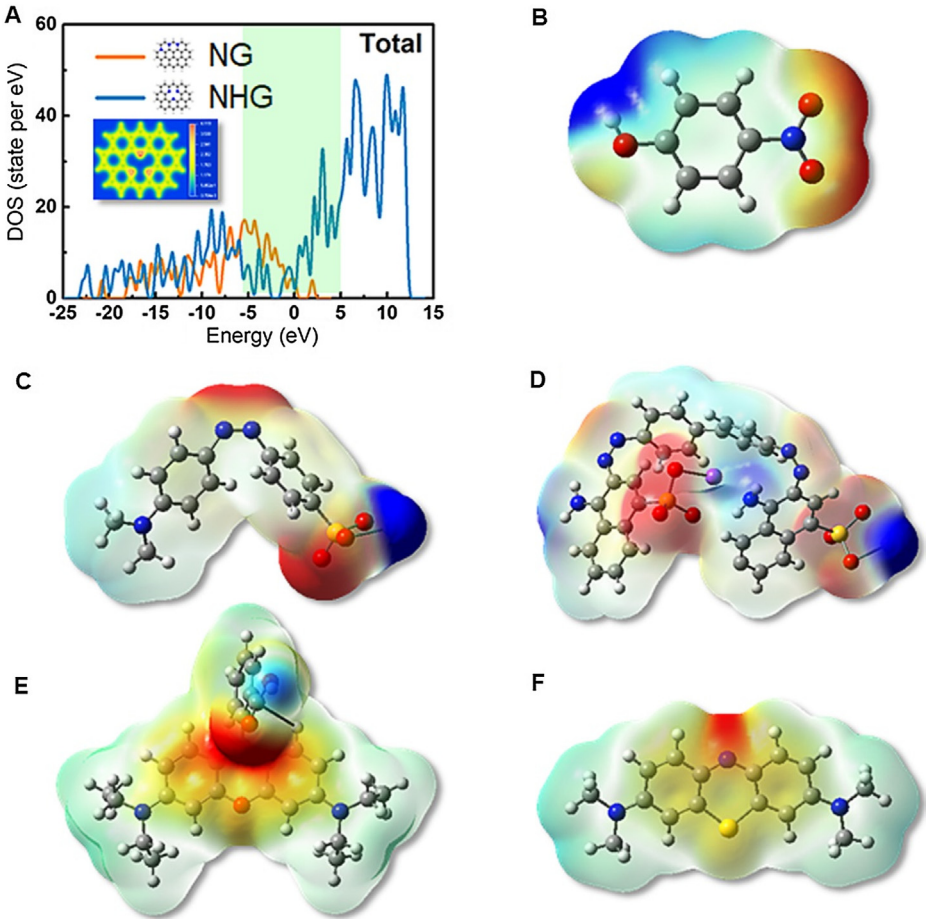


**Fig. 6.** (A) Total DOS (state per eV) of NG and NHG, inset is electron density mapping diagram of NHG; Electrostatic potential distribution of (B) 4-NP, (C) MO, (D) CR, (E) RhB and (F) MB.

## 4. Conclusion

In summary, we report a facile one-pot, and effective synthesis approach to synthesize NHG through hydrothermal treatment of GO in the presence of ammonium hydroxide and hydrogen peroxide. The graphene oxide sheets can simultaneously be reduced, self-assembled, chemically etched and nitrogen doped into monolithic NHG hydrogel and then finally converted into NHG suspension. The metal-free carbocatalyst prepared with this method had a 3D macroporous framework, hydrophilic property, large SSA (322.1 $m^2 g^{-1}$) and hierarchical mesoporous structure, as well as high content of doped N element (9.77 at. %). Owing to the excellent properties, NHG exhibited a high activity toward the catalytic hydrogenation of five different organic dyes in aqueous solution. Furthermore, the nitrobenzenes reduction reactions were implemented with very high efficiency catalyzed by NHG. These hydrogenation reactions were found to proceed at room temperature and afforded the desired product in excellent yields. Typically, the TOF for 4-NP reduction ($3.32 \times 10^{-2}$ $min^{-1}$) was higher than that of commercial Pd/C (5.0 wt%) and those gained by carbocatalysts which have been reported in literatures. Molecular structure analysis combined with theoretical calculations elucidated the metal-free catalytic mechanism. Based on the obtained results, it is envisioned that the NHG carbocatalyst has great potential applications in organic catalysis and wastewater treatment.

## Author contributions

J.B. Xi conceived the idea. Z.L. He, J. Liu, M. Zhao, Z.P. Wen, C.Y. Xie and J. Chen carried out the materials synthesis and the chemical catalysis. Q.J. Wang and C.Y. Tang performed the DFT calculation. J.B. Xi and Z.L. He performed the materials characterizations. The manuscript was written through contributions of all authors. All authors have given approval to the final version of the manuscript. §Z.L. He, J. Liu, Q.J. Wang and M. Zhao contributed equally.

## Declaration of Competing Interest

The authors declare no competing financial interest.

## Acknowledgements

This research was financially supported by the Natural Science Foundation of Hubei Province (Nos. 2016CFB263, 2016CFB168 and 2018CFB159) and the National Natural Science Foundation of China (Nos. 21702155, 51772110 and 51708427). The authors would like to acknowledge the Analytical and Testing Center of Huazhong University of Science and Technology and the Wuhan National Laboratory for Optoelectronics for SEM, TEM, XPS and Raman measurements. The authors also would like to show great

gratitude to Multi-function Computer Center of Guangxi University for the computational resources.

## Appendix A. Supplementary material

Supplementary data to this article can be found online at https://doi.org/10.1016/j.jcat.2019.07.017.

## References

[1] A. Bafana, S. Devi, T. Chakrabarti, Environ. Rev. 19 (2011) 350–371.
[2] Z.P. Wen, Y.L. Zhang, G. Cheng, Y.R. Wang, R. Chen, Chemosphere 218 (2019) 1002–1013.
[3] H. Wang, L.F. Liang, X.J. Cheng, Y.M. Luo, S. Sun, Photochem. Photobiol. 94 (2018) 17–26.
[4] Z. Ulma, E. Rahayuningsih, T.D. Wahyuningsih, IOP conference series: materials science and engineering, IOP Publishing 299 (2018) 012075.
[5] P. Singh, S. Roy, A. Jaiswal, J. Phys. Chem. C 121 (2017) 22914–22925.
[6] Y.M. Slokar, A. Majcen Le Marechal, Dyes Pigm. 37 (1998) 335–356.
[7] J.B. Xi, H.Y. Sun, D. Wang, Z.Y. Zhang, X.M. Duan, J.W. Xiao, F. Xiao, L.M. Liu, S. Wang, Appl. Catal. B- Environ. 225 (2018) 291–297.
[8] R.F. Nie, M. Miao, W.C. Du, J.J. Shi, Y.C. Liu, Z.Y. Hou, Appl. Catal. B- Environ. 180 (2016) 607–613.
[9] Y.J. Sun, J.Z. Jiang, Y. Liu, S.L. Wu, J. Zou, Appl. Surf. Sci. 430 (2018) 362–370.
[10] F.X. Chen, S.L. Xie, X.L. Huang, X.H. Qiu, J. Hazard. Mater. 322 (2017) 152–162.
[11] J. Ke, J. Liu, H.Q. Sun, H.Y. Zhang, X.G. Duan, P. Liang, X.Y. Li, M.O. Tadé, S.M. Liu, S.B. Wang, Appl. Catal. B- Environ. 200 (2017) 47–55.
[12] V.C. Bhethanabotla, D.R. Russell, J.N. Kuhn, Appl. Catal. B- Environ. 202 (2017) 156–164.
[13] F. He, J.Q. Luo, S.T. Liu, Chem. Eng. J. 294 (2016) 362–370.
[14] L.M. Dai, Y.H. Xue, L.T. Qu, H.J. Choi, J.B. Baek, Chem. Rev. 115 (2015) 4823–4892.
[15] L. Miao, D.Z. Zhu, M.X. Liu, H. Duan, Z.W. Wang, Y.K. Lv, W. Xiong, Q.J. Zhu, L.C. Li, X.L. Chai, L.H. Gan, Chem. Eng. J. 347 (2018) 233–242.
[16] J. Yu, Y.Y. Zhang, H. Li, Q.J. Wan, Y.W. Li, N.J. Yang, Carbon 129 (2018) 301–339.
[17] M. Liu, Q. Guan, S.T. Liu, Ionics 24 (2018) 2783–2793.
[18] X.G. Duan, H.Q. Sun, Y.X. Wang, J. Kang, S.B. Wang, ACS Catal. 5 (2015) 553–559.
[19] D.R. Dreyer, H.P. Jia, C.W. Bielawski, Angew. Chem. Int. Ed. 49 (2010) 6813–6816.
[20] C.L. Su, M. Acik, K. Takai, J. Lu, S.J. Hao, Y. Zheng, P.P. Wu, Q.L. Bao, T. Enoki, Y.J. Chabal, K.P. Loh, Nat. Commun. 3 (2012) 1298.
[21] H.Q. Sun, S.Z. Liu, G.L. Zhou, H.M. Ang, M.O. Tadé, S.B. Wang, A.C.S. Appl, Mater. Interfaces 4 (2012) 5466–5471.
[22] X.G. Duan, H.Q. Sun, S.B. Wang, Metal-Free carbocatalysis in advanced oxidation reactions, Accounts Chem. Res. 51 (2018) 678–687.
[23] B. Frank, J. Zhang, R. Blume, R. Schlogl, D.S. Su, Angew. Chem. Int. Ed. 48 (2009) 6913–6917.
[24] P.W. Gong, J.Y. Du, D.D. Wang, B.B. Cao, M. Tian, Y.H. Wang, L. Sun, S.J. Ji, Z. Liu, J. Mater. Chem. B 6 (2018) 2769–2777.
[25] X.K. Kong, Z.Y. Sun, M. Chen, C.L. Chen, Q.W. Chen, Energy Environ. Sci. 6 (2013) 3260–3266.
[26] J.B. Xi, Q.J. Wang, J. Liu, L. Huan, Z.L. He, Y. Qiu, J. Zhang, C.Y. Tang, J. Xiao, S. Wang, J. Catal. 359 (2018) 233–241.
[27] Y.Y. Shao, S. Zhang, M.H. Engelhard, G.S. Li, G. Shao, Y. Wang, J. Liu, I.A. Aksay, Y.H. Lin, J. Mater. Chem. 20 (2010) 7491–7496.
[28] B.M. Wei, Z.W. Zhai, H.B. Wang, J.T. Zhang, C.Z. Xu, Y.L. Xu, L. He, D. Xie, J. Agric. Food Chem. 66 (2018) 9080–9086.
[29] Jr W.S. Hummers, R.E. Offeman, J. Am. Chem. Soc. 8 (1958) 1339–1339.
[30] M.J. Frisch, G.W. Trucks, H.B. Schlegel, G.E. Scuseria, M.A. Robb, J.R. Cheeseman, H. Nakatsuji, et al., Gaussian 09, Revision A.02, Gaussian, Inc, Wallingford, CT, 2009.
[31] F. Weigenda, R. Ahlrichs, Phys. Chem. Chem. Phys. 7 (2005) 3297–3305.
[32] S.A. Carabineiro, R.M. Bellabarba, P.T. Gomes, S.I. Pascu, L.F. Veiros, C. Freire, L. C.J. Pereira, R.T. Henriques, M.C. Oliveira, J.E. Warren, Inorg. Chem. 47 (2008) 8896–8911.
[33] J. Autschbach, T. Ziegler, S.J.A. van Gisbergen, E.J. Baerends, J. Chem. Phys. 116 (2002) 6930–6940.
[34] X.P. Wang, L.X. Lv, Z.H. Cheng, J. Gao, L.Y. Dong, C.G. Hu, L.T. Qu, Adv. Energy Mater. 6 (2016) 150210.
[35] J.W. Jang, C.E. Lee, S.C. Lyu, T.J. Lee, C.J. Lee, Appl. Phys. Lett. 84 (2004) 2877–2879.
[36] X.L. Li, H.L. Wang, J.T. Robinson, H. Sanchez, G. Diankov, H.J. Dai, J. Am. Chem. Soc. 131 (2009) 15939–15944.
[37] J.B. Xi, Y. Zhang, Q.J. Wang, J. Xiao, K. Chi, X.M. Duan, J. Chen, C.Y. Tang, Y.M. Sun, F. Xiao, S. Wang, Sensor Actuat. B-Chem. 273 (2018) 108–117.
[38] J.T. Xu, Y. Lin, J.W. Connell, L.M. Dai, Small 11 (2015) 6179–6185.
[39] Q.J. Wang, S. Zhou, S. Xiao, F.F. Wei, X.Z. Zhao, J.E. Qu, H.R. Wang, RSC Adv. 8 (2018) 14775–14786.
[40] S.L. Yang, C.Y. Cao, Y.B. Sun, P.P. Huang, F.F. Wei, W.G. Song, Angew. Chem. 127 (2015) 2699–2702.
[41] B. Naik, S. Hazra, V.S. Prasad, N.N. Ghosh, Catal. Commun. 12 (2011) 1104–1108.
[42] A. Hernández-Gordillo, A.G. Romero, F. Tzompantzi, S. Oros-Ruiz, R.J. Gómez, Photochem. Photobio. A: Chem. 257 (2013) 44–49.
[43] F. Wang, S.Y. Song, K. Li, J.Q. Li, J. Pan, S. Yao, X. Ge, J. Feng, X. Wang, H.J. Zhang, Adv. Mater. 28 (2016) 10679–10683.
[44] F. Yang, C. Chi, C.X. Wang, Y. Wang, Y.F. Li, Green Chem. 18 (2016) 4254–4262.
[45] H.W. Hu, J.H. Xin, H. Hu, X.W. Wang, Nano Res. 8 (2015) 3992–4006.
[46] H.W. Hu, X.W. Wang, D.G. Miao, Y.F. Wang, C.L. Lai, Y.J. Guo, W.Y. Wang, J.H. Xin, H. Hu, Chem. Commun. 51 (2015) 16699–16702.
[47] W. Zhou, Y. Zhou, Y. Liang, X.H. Feng, H. Zhou, RSC Adv. 5 (2015) 50505–50511.
[48] J.B. Xi, J.W. Xiao, F. Xiao, Y.X. Jin, Y. Dong, J. Feng, S. Wang, Sci. Rep. 6 (2016) 21904.
[49] X.M. Duan, M.C. Xiao, S. Liang, Z.Y. Zhang, Y. Zeng, J.B. Xi, S. Wang, Carbon 30 (2018) 806–813.
[50] X.M. Duan, J. Liu, J.F. Hao, L.M. Wu, B.J. He, Y. Qiu, J. Zhang, Z.L. He, J.B. Xi, S. Wang, Carbon 130 (2018) 806–813.
[51] J. Liu, J.F. Hao, C.C. Hu, B.J. He, J.B. Xi, J.W. Xiao, S. Wang, Z.W. Bai, J. Phsy. Chem. C 122 (2018) 2696–2703.
[52] T. Sun, Z.Y. Zhang, J.W. Xiao, C. Chen, F. Xiao, S. Wang, Y.Q. Liu, Sci. Rep. 3 (2013) 2527.
[53] F. Hu, M. Patel, F.X. Luo, C. Flach, R. Mendelsohn, E. Garfunkel, H.X. He, M. Szostak, J. Am. Chem. Soc. 137 (2015) 14473–14480.
[54] S.K. Lee, A. Mills, Chem. Commun. 18 (2003) 2366–2367.